

Quantum transport through a double Aharonov-Bohm-interferometer in the presence of Andreev reflection

Yong-Ping Zhang, Hui Yu, Ying-Fang Gao, J. -Q. Liang
*Institute of Theoretical Physics, Shanxi
 University, Taiyuan, Shanxi, 030006, China*

Quantum transport through a double Aharonov-Bohm-interferometer in the presence of Andreev reflection is investigated in terms of the nonequilibrium Green function method with which the reflection current is obtained. Tunable Andreev reflection probabilities depending on the interdot coupling strength and magnetic flux as well are analysed in detail. It is found that the oscillation period of the reflection probability with respect to the magnetic flux for the double interferometer depends linearly on the ratio of two parts magnetic fluxes n , i.e. $2(n+1)\pi$, while that of a single interferometer is 2π . The coupling strength not only affects the height and the linewidth of Andreev reflection current peaks vs gate voltage but also shifts the peak positions. It is furthermore demonstrated that the Andreev reflection current peaks can be tuned by the magnetic fluxes.

PACS: 73.23.-b; 74.45.+c; 73.63.Kv

I. INTRODUCTION

Quantum dots (QDs) containing discrete energy levels which can be tuned easily in experiment have been attracting considerable attention continuously, and the study of quantum transport properties through QDs has become an interesting field which serves as a testing ground for the physical phenomena, such as Kondo [1,2] and Fano effects [3]. Recent developments on the study include Coulomb on-site repulsion [4], spin-flip effect caused by the magnetic leads [5] or rotating magnetic field [6], and phonon-assisted tunneling in the molecular QD [7] with time-dependent field or ac gate voltage [8,9].

Electron transports coherently through an open QD can be investigated in the standard procedure by means of nonequilibrium Green function (NGF) [8], the rate equation [10] and some other methods [11]. The current characteristic properties change dramatically if the QD is connected to additional devices, so various kinds of hybrid QD systems have been studied in the literature. Two aspects mainly involved in those hybrid systems are the ferromagnetic and superconductor properties which evoke the spin degree of freedom of electrons. The F-QD-F system, i.e., QD coupled with two ferromagnetic leads, has been studied as spin-valve device [5,12]. In the superconductor case, the Andreev reflection, conserving the momentum of the reflected particle but not the charge, plays a dominant role at the interface between a normal metal and a superconductor. Using multichannel S-matrix method, Beenakker demonstrated the resonant Andreev tunneling in the normal metal-normal QD-superconductor (N-NQD-S) hybrid system in the zero-bias limit [13]; later Claughton et al. extended this theory to the finite-bias case [14]. Sun et al. explored the resonant Andreev reflection in this system with multienergy levels in normal QD and found that some extra peaks originating from the Andreev reflection superimposed on the conventional current plateaus [15]. And they also investigated the photon-assisted Andreev and normal tunnels in this system. With an applied time-varying external field, it was observed that a series of photon-assisted Andreev tunneling peaks appeared in the curve of the average current $\langle I \rangle$ vs the gate voltage with the negative peaks on the left-hand side and positive peaks on the right-hand side of the original resonant peak in the absence of the external field [16]. Another interesting hybrid system consists of ferromagnet and superconductor leads coupled with a normal QD (F-QD-S). In Ref. [17], Zhu et al. provided an efficient method for introducing a spin degree of freedom in this system, and also derived the general current formula of the Andreev reflection in a quantum dot connected with two ferromagnetic and one superconductor leads (F_1, F_2 -QD-S) [18]. Considering both the Coulomb interaction and the multienergy levels in QD, Feng and Xiong studied the transport properties in the F-QD-S system [19]. Very recently, Cao et al. considered the spin-flip effect in QD of a F-QD-S system and found that the single-resonance peak of the Andreev reflection conductance versus the gate voltage would spill into a double-resonance peak with the increasing of the spin-flip scattering strength [20]. Thus far, most of studies relating to Andreev reflection have been focused on a single-QD system.

On the other hand, the electron transport through a double-quantum-dot (DQD), especially the parallel-coupled double-quantum-dot (PDQD), is an interesting subject which may involve the quantum phase interference. An open PDQD threaded by a magnetic flux is regarded as an Aharonov-Bohm (AB) interferometer in which the coherence of the electron remains partly even in the presence of Coulomb repulsion [1,21]. Tunable coupling strength between two parallel dots makes the transport properties more complex and interesting [22,23]. The tunable Andreev reflection in an AB interferometer has been investigated recently by Peng et al. [25].

In this paper we shall study the electron transport through a N-PDQD-S structure, i.e., a parallel-coupled double-quantum dot that is connected with two leads, one is a normal metal and the other is a superconductor. The device threaded by two magnetic fluxes (see Fig.1) with the interdot coupling can be regarded as a double AB interferometer. By using the NGF method, the current J_L and the probability of the Andreev reflection are derived.

The paper is organized as follows: In Sec. II, we present the model Hamiltonian and derive the general formula of the current and the probability of the Andreev reflection with NGF method. In Sec. III, the properties of the current due to Andreev reflection depending on bias voltage, magnetic flux, gate voltage, and interdot coupling strength are studied in detail, and several different effects are predicted. Finally, a brief summary is given in Sec. IV.

II. MODEL HAMILTONIAN AND FORMULATION

The Hamiltonian of the system schematically shown in Fig. 1 can be decomposed into four parts of the following form:

$$H = H_L + H_R + H_D + H_T, \quad (1)$$

where

$$\begin{aligned} H_L &= \sum_{k\sigma} (\varepsilon_k - eV) a_{k\sigma}^\dagger a_{k\sigma}, \\ H_R &= \sum_{p\sigma} \varepsilon_p b_{p\sigma}^\dagger b_{p\sigma} + \sum_p (\Delta b_{p\downarrow} b_{-p\uparrow} + h.c.), \\ H_D &= \sum_{\sigma, i=1,2} \varepsilon_i d_{i\sigma}^\dagger d_{i\sigma} + \sum_{\sigma} (\Omega e^{i\Phi_{12}} d_{2\sigma}^\dagger d_{1\sigma} + h.c.), \\ H_T &= \sum_{k\sigma, i=1,2} (L_i e^{i\Phi_{iL}} a_{k\sigma}^\dagger d_{i\sigma} + h.c.) \\ &\quad + \sum_{p\sigma, i=1,2} (R_i e^{i\Phi_{iR}} b_{p\sigma}^\dagger d_{i\sigma} + h.c.). \end{aligned} \quad (2)$$

H_L describes the left normal metal lead, $a_{k\sigma}$ ($a_{k\sigma}^\dagger$) is the corresponding annihilation (creation) operator, and V is the bias voltage. We assume the chemical potential of right lead $\mu_R = 0$ [16]. H_R describes the right superconductor lead with the energy gap Δ . H_D models the coupled double quantum dots, Ω is the interdot coupling strength, and Φ_{12} is the corresponding phase shift induced by the magnetic flux. Here we consider the single energy level in each quantum dot. H_T is the tunneling part of Hamiltonian, L_i (R_i), independent of momentum k (p), is the hopping strength between i th quantum dot [i. e. the quantum dot with energy level ε_i ($i = 1, 2$)] and left (right) lead, and Φ_{L1} is the phase shift of the electron tunneling from the left lead to first quantum dot, where

$$\Phi_{L1} = \Phi_{1R} = \frac{\Phi}{4}$$

where $\Phi = 2\pi(\alpha_1 + \alpha_2)$ with $\Phi_i = \alpha_i \Phi_0$ ($i = 1, 2$) being the magnetic flux in the quantum unit $\Phi_0 = hc/e$ and $\Phi_{12} = -\Phi_{21} = 2\pi(\alpha_1 - \alpha_2)$.

The current from the left lead to a quantum dot can be written as [4,8]

$$\begin{aligned} J_L(t) &= -\frac{2e}{\hbar} \text{Im} \int d\varepsilon \sum_{i,j=1,2} \sum_{k\sigma} L_i L_j^* e^{i(\Phi_{iL} + \Phi_{Lj})} \\ &\quad \times \delta(\varepsilon - \varepsilon_k) \int_{-\infty}^{\infty} dt_1 [G_{ij\sigma}^r(t, t_1) f_L(\varepsilon + eV) \\ &\quad + \theta(t' - t_1) G_{ij\sigma}^<(t, t_1)] e^{-i\varepsilon(t_1 - t')}, \end{aligned} \quad (3)$$

where we define $G_{ij\sigma}^r(t, t') = -i\theta(t - t') \langle \{d_{i\sigma}(t), d_{j\sigma}^\dagger(t')\} \rangle$ and $G_{ij\sigma}^<(t, t') = i \langle d_{j\sigma}^\dagger(t') d_{i\sigma}(t) \rangle$. Because of the right superconductor lead, it is convenient to introduce 4×4 matrix representation in which $\mathbf{G}^r(t, t')$ and $\mathbf{G}^<(t, t')$ have the forms,

$$\mathbf{G}^r(t, t') \equiv -i\theta(t - t') \langle \{ \Psi(t), \Psi^\dagger(t') \} \rangle, \quad (4)$$

$$\mathbf{G}^<(t, t') \equiv i \langle \Psi^\dagger(t') \Psi(t) \rangle, \quad (5)$$

where $\Psi^\dagger = (d_{1\uparrow}^\dagger, d_{1\downarrow}, d_{2\uparrow}^\dagger, d_{2\downarrow})$. So Eq. (3) can be rewritten as

$$J_{L\uparrow}(t) = -\frac{2e}{\hbar} \text{Im} \int \frac{d\varepsilon}{2\pi} \int_{-\infty}^t dt' e^{-i\varepsilon(t-t')} \{ \Gamma^L [\mathbf{G}^r(t, t') f_L(\varepsilon + eV) + \mathbf{G}^<(t, t')] \}_{11+33}, \quad (6)$$

where

$$\begin{aligned} \Gamma^L &= 2\pi \sum_k \delta(\varepsilon - \varepsilon_k) \begin{pmatrix} L_1 L_1^* & 0 & L_2 L_1^* e^{i\frac{\Phi}{2}} & 0 \\ 0 & L_1 L_1^* & 0 & L_1 L_2^* e^{-i\frac{\Phi}{2}} \\ L_1 L_2^* e^{-i\frac{\Phi}{2}} & 0 & L_2 L_2^* & 0 \\ 0 & L_2 L_1^* e^{i\frac{\Phi}{2}} & 0 & L_2 L_2^* \end{pmatrix} \\ &= \begin{pmatrix} \Gamma_1^L & 0 & \sqrt{\Gamma_1^L \Gamma_2^L} e^{i\frac{\Phi}{2}} & 0 \\ 0 & \Gamma_1^L & 0 & \sqrt{\Gamma_1^L \Gamma_2^L} e^{-i\frac{\Phi}{2}} \\ \sqrt{\Gamma_1^L \Gamma_2^L} e^{-i\frac{\Phi}{2}} & 0 & \Gamma_2^L & 0 \\ 0 & \sqrt{\Gamma_1^L \Gamma_2^L} e^{i\frac{\Phi}{2}} & 0 & \Gamma_2^L \end{pmatrix}. \end{aligned} \quad (7)$$

with $\Gamma_1^L = 2\pi \sum_k \delta(\varepsilon - \varepsilon_k) L_1 L_1^*$, $\Gamma_2^L = 2\pi \sum_k \delta(\varepsilon - \varepsilon_k) L_2 L_2^*$, here we consider only a spin-up current $J_{L\uparrow}(t)$ [$J_{L\downarrow}(t)$ is easily obtained from $J_{L\uparrow}(t)$ by exchanging the spin index].

To calculate $\mathbf{G}^r(t, t')$, we start from the Dyson equation,

$$\mathbf{G}^r(t, t') = \mathbf{g}^r(t, t') + \int dt_1 dt_2 \mathbf{G}^r(t, t_1) \boldsymbol{\Sigma}^r(t_1, t_2) \mathbf{g}^r(t_2, t'), \quad (8)$$

in which $\mathbf{g}^r(t, t')$ is the retarded Green function for the isolated quantum dots, and can be easily obtained as,

$$\mathbf{g}^r(t, t') = -i\theta(t-t') \begin{pmatrix} e^{-i\varepsilon_1(t-t')} & 0 & 0 & 0 \\ 0 & e^{i\varepsilon_1(t-t')} & 0 & 0 \\ 0 & 0 & e^{-i\varepsilon_2(t-t')} & 0 \\ 0 & 0 & 0 & e^{i\varepsilon_2(t-t')} \end{pmatrix}. \quad (9)$$

Self-energy $\boldsymbol{\Sigma}^r(t_1, t_2)$ consists of three parts, such that,

$$\boldsymbol{\Sigma}^r(t_1, t_2) = \boldsymbol{\Sigma}_{12} + \boldsymbol{\Sigma}_L^r(t_1, t_2) + \boldsymbol{\Sigma}_R^r(t_1, t_2), \quad (10)$$

where $\boldsymbol{\Sigma}_L^r(t_1, t_2)$ results from the tunneling coupling between QD and the normal metal lead, $\boldsymbol{\Sigma}_R^r(t_1, t_2)$ between QD and superconductor lead, and $\boldsymbol{\Sigma}_{12}$ is from interdot coupling contribution. Under the wide-bandwidth approximation [8,16,20], the self-energy becomes

$$\boldsymbol{\Sigma}_{12} = \begin{pmatrix} 0 & 0 & \Omega^* e^{-i\Phi_{12}} & 0 \\ 0 & 0 & 0 & -\Omega e^{i\Phi_{12}} \\ \Omega e^{i\Phi_{12}} & 0 & 0 & 0 \\ 0 & -\Omega^* e^{-i\Phi_{12}} & 0 & 0 \end{pmatrix}, \quad (11)$$

and $\boldsymbol{\Sigma}_L^r(t_1, t_2)$ is written as

$$\begin{aligned} \boldsymbol{\Sigma}_L^r(t_1, t_2) &= \sum_k \mathbf{L}^* \mathbf{g}_k^r(t_1, t_2) \mathbf{L} \\ &= -\frac{i}{2} \delta(t_1 - t_2) \boldsymbol{\Gamma}^L, \end{aligned} \quad (12)$$

where

$$\mathbf{L} = \begin{pmatrix} L_1 e^{-i\frac{\Phi}{4}} & 0 & 0 & 0 \\ 0 & -L_1^* e^{i\frac{\Phi}{4}} & 0 & 0 \\ 0 & 0 & L_2 e^{i\frac{\Phi}{4}} & 0 \\ 0 & 0 & 0 & -L_2^* e^{-i\frac{\Phi}{4}} \end{pmatrix}. \quad (13)$$

The self-energy from the coupling between QD and right superconductor lead is given by [16],

$$\begin{aligned}
& \Sigma_R^r(t_1, t_2) \\
&= \sum_p \mathbf{R}^* \mathbf{g}_p^r(t_1, t_2) \mathbf{R} \\
&= -i\theta(t_1 - t_2) \\
& \times \int \frac{d\varepsilon}{2\pi} \frac{e^{-i\varepsilon(t-t')} |\varepsilon|}{\sqrt{\varepsilon^2 - \Delta^2}} \begin{pmatrix} \Gamma_1^R & -\Gamma_1^R e^{-i\frac{\Phi}{2}} \frac{\Delta}{|\varepsilon|} & \sqrt{\Gamma_1^R \Gamma_2^R} e^{-i\frac{\Phi}{2}} & -\sqrt{\Gamma_1^R \Gamma_2^R} \frac{\Delta}{|\varepsilon|} \\ -\Gamma_1^R e^{i\frac{\Phi}{2}} \frac{\Delta}{|\varepsilon|} & \Gamma_1^R & -\sqrt{\Gamma_1^R \Gamma_2^R} \frac{\Delta}{|\varepsilon|} & \sqrt{\Gamma_1^R \Gamma_2^R} e^{i\frac{\Phi}{2}} \\ \sqrt{\Gamma_1^R \Gamma_2^R} e^{i\frac{\Phi}{2}} & -\sqrt{\Gamma_1^R \Gamma_2^R} \frac{\Delta}{|\varepsilon|} & \Gamma_2^R & -\Gamma_2^R e^{i\frac{\Phi}{2}} \frac{\Delta}{|\varepsilon|} \\ -\sqrt{\Gamma_1^R \Gamma_2^R} \frac{\Delta}{|\varepsilon|} & \sqrt{\Gamma_1^R \Gamma_2^R} e^{-i\frac{\Phi}{2}} & -\Gamma_2^R e^{-i\frac{\Phi}{2}} \frac{\Delta}{|\varepsilon|} & \Gamma_2^R \end{pmatrix},
\end{aligned} \tag{14}$$

where

$$\mathbf{R} = \begin{pmatrix} R_1 e^{i\frac{\Phi}{4}} & 0 & 0 & 0 \\ 0 & -R_1^* e^{-i\frac{\Phi}{4}} & 0 & 0 \\ 0 & 0 & R_2 e^{-i\frac{\Phi}{4}} & 0 \\ 0 & 0 & 0 & -R_2^* e^{i\frac{\Phi}{4}} \end{pmatrix}, \tag{15}$$

and the retarded Green function of the isolated superconductor lead $g_p^r(t, t')$ is read as

$$\mathbf{g}_p^r(t, t') = -i\theta(t - t') \int d\varepsilon \rho_R^N \frac{e^{-i\varepsilon(t-t')} |\varepsilon|}{\sqrt{\varepsilon^2 - \Delta^2}} \begin{pmatrix} 1 & \frac{\Delta}{|\varepsilon|} & 1 & \frac{\Delta}{|\varepsilon|} \\ \frac{\Delta}{|\varepsilon|} & 1 & \frac{\Delta}{|\varepsilon|} & 1 \\ 1 & \frac{\Delta}{|\varepsilon|} & 1 & \frac{\Delta}{|\varepsilon|} \\ \frac{\Delta}{|\varepsilon|} & 1 & \frac{\Delta}{|\varepsilon|} & 1 \end{pmatrix}. \tag{16}$$

with ρ_R^N being the density states of the right lead in a normal metal state. We define $\Gamma_1^R = 2\pi |R_1|^2 \rho_R^N$. By substituting Eqs. (9)–(13) into Eq. (8), the Green function $\mathbf{G}^r(t, t')$ can be derived. It is, however, convenient to transform Eq. (8) into the energy representation by making use of the Fourier transformation,

$$\mathbf{G}^r(E, E') = \int dt dt' \mathbf{G}^r(t, t') e^{iEt} e^{-iE't'}. \tag{17}$$

Then solving Eq. (8) in the energy representation, we get (see Appendix A)

$$G_{ij}^r(E, E') = 2\pi \tilde{G}_{ij}^r(E') \delta(E - E'), \tag{18}$$

here, $i, j = 1, 2, 3, 4$. $G_{ij}^r(E, E')$ are the elements of the matrix $\mathbf{G}^r(E, E')$, and the detailed calculation of $\tilde{G}_{ij}^r(E')$ is given in Appendix A. The Green function $\mathbf{G}^r(t, t')$ is obtained after making an inverse Fourier transformation as

$$\mathbf{G}^r(t, t') = \frac{1}{(2\pi)^2} \int dE dE' \mathbf{G}^r(E, E') e^{-iEt} e^{iE't'}. \tag{19}$$

In the following, we derive the smaller Green function using the Keldysh equation

$$\mathbf{G}^<(t, t') = \int dt_1 dt_2 \mathbf{G}^r(t, t_1) \mathbf{\Sigma}^<(t_1, t_2) \mathbf{G}^a(t_2, t'), \tag{20}$$

where,

$$\mathbf{\Sigma}^<(t_1, t_2) = \mathbf{\Sigma}_L^<(t_1, t_2) + \mathbf{\Sigma}_R^<(t_1, t_2), \tag{21}$$

with

$$\begin{aligned}
& \Sigma_L^<(t_1, t_2) \\
&= \sum_k \mathbf{L}^* \mathbf{g}_k^<(t_1, t_2) \mathbf{L} \\
&= i \int \frac{d\varepsilon}{2\pi} e^{-i\varepsilon(t_1-t_2)} \begin{pmatrix} f_L(\varepsilon + eV) & 0 & 0 & 0 \\ 0 & f_L(\varepsilon - eV) & 0 & 0 \\ 0 & 0 & f_L(\varepsilon + eV) & 0 \\ 0 & 0 & 0 & f_L(\varepsilon - eV) \end{pmatrix} \mathbf{\Gamma}^L, \tag{22}
\end{aligned}$$

and

$$\begin{aligned}
\Sigma_R^<(t_1, t_2) &= \sum_p \mathbf{R}^* \mathbf{g}_p^<(t_1, t_2) \mathbf{R} \\
&= i \int \frac{d\varepsilon}{2\pi} e^{-i\varepsilon(t_1-t_2)} f_R(\varepsilon) \tilde{\rho}_R(\varepsilon) \\
&\quad \times \begin{pmatrix} \Gamma_1^R & -\Gamma_1^R e^{-i\frac{\Phi}{2}} \frac{\Delta}{|\varepsilon|} & \sqrt{\Gamma_1^R \Gamma_2^R} e^{-i\frac{\Phi}{2}} & -\sqrt{\Gamma_1^R \Gamma_2^R} \frac{\Delta}{|\varepsilon|} \\ -\Gamma_1^R e^{i\frac{\Phi}{2}} \frac{\Delta}{|\varepsilon|} & \Gamma_1^R & -\sqrt{\Gamma_1^R \Gamma_2^R} \frac{\Delta}{|\varepsilon|} & \sqrt{\Gamma_1^R \Gamma_2^R} e^{i\frac{\Phi}{2}} \\ \sqrt{\Gamma_1^R \Gamma_2^R} e^{i\frac{\Phi}{2}} & -\sqrt{\Gamma_1^R \Gamma_2^R} \frac{\Delta}{|\varepsilon|} & \Gamma_2^R & -\Gamma_2^R e^{i\frac{\Phi}{2}} \frac{\Delta}{|\varepsilon|} \\ -\sqrt{\Gamma_1^R \Gamma_2^R} \frac{\Delta}{|\varepsilon|} & \sqrt{\Gamma_1^R \Gamma_2^R} e^{-i\frac{\Phi}{2}} & -\Gamma_2^R e^{-i\frac{\Phi}{2}} \frac{\Delta}{|\varepsilon|} & \Gamma_2^R \end{pmatrix}, \tag{23}
\end{aligned}$$

where

$$\tilde{\rho}_R(\varepsilon) = \frac{|\varepsilon| \theta(|\varepsilon| - \Delta)}{\sqrt{\varepsilon^2 - \Delta^2}}. \tag{24}$$

$\tilde{\rho}_R(\varepsilon)$ is the ratio of superconducting density of states to the normal density of states [15]. According to Eq. (20), $\mathbf{G}^<(t, t)$ can be obtained by substituting Eqs. (21)-(23) and the Green functions $\mathbf{G}^r(t_1, t_2)$, $\mathbf{G}^a(t_1, t_2)$ into Eq. (20) with the results of matrix elements $G_{11}^<(t, t)$, $G_{13}^<(t, t)$, $G_{31}^<(t, t)$, and $G_{33}^<(t, t)$ shown in Appendix B.

The total current, i.e., the sum of both spin-up and spin-down parts, is found by substituting the retarded Green function $G_{ij}^r(t, t')$ and the smaller Green function $G_{ij}^<(t, t)$ shown in Appendix B into Eq. (6), and the result is

$$J_L = J_A + J_T \tag{1}$$

where

$$J_A = \frac{2e}{\hbar} \int \frac{d\varepsilon}{2\pi} [f_L(\varepsilon + eV) - f_L(\varepsilon - eV)] T_{AR},$$

and

$$J_T = \frac{2e}{\hbar} \int \frac{d\varepsilon}{2\pi} [f_L(\varepsilon + eV) - f_R(\varepsilon)] \tilde{\rho}_R(\varepsilon) T_{LR}.$$

J_A is seen to be the current due to the Andreev reflection contribution and the probability of the Andreev reflection T_{AR} is given by

$$\begin{aligned}
T_{AR} &= (\Gamma_1^L)^2 \left| \tilde{G}_{12}^r(\varepsilon) \right|^2 + (\Gamma_2^L)^2 \left| \tilde{G}_{34}^r(\varepsilon) \right|^2 \\
&\quad + \Gamma_1^L \Gamma_2^L \left(\left| \tilde{G}_{14}^r(\varepsilon) \right|^2 + \left| \tilde{G}_{32}^r(\varepsilon) \right|^2 \right) \\
&\quad + 2\sqrt{\Gamma_1^L \Gamma_2^L} \operatorname{Re}[\Gamma_1^L e^{-i\frac{\Phi}{2}} \tilde{G}_{12}^r(\varepsilon) \tilde{G}_{14}^{r*}(\varepsilon) \\
&\quad + \Gamma_2^L e^{-i\frac{\Phi}{2}} \tilde{G}_{32}^r(\varepsilon) \tilde{G}_{34}^{r*}(\varepsilon) + \Gamma_1^L e^{-i\frac{\Phi}{2}} \tilde{G}_{12}^r(\varepsilon) \tilde{G}_{32}^{r*}(\varepsilon) \\
&\quad + \sqrt{\Gamma_1^L \Gamma_2^L} e^{-i\Phi} \tilde{G}_{12}^r(\varepsilon) \tilde{G}_{34}^{r*}(\varepsilon) + \sqrt{\Gamma_1^L \Gamma_2^L} \tilde{G}_{14}^r(\varepsilon) \tilde{G}_{32}^{r*}(\varepsilon) \\
&\quad + \Gamma_2^L e^{-i\frac{\Phi}{2}} \tilde{G}_{14}^r(\varepsilon) \tilde{G}_{34}^{r*}(\varepsilon)]. \tag{26}
\end{aligned}$$

As explained in Refs. [15,24], the term $(\Gamma_1^L)^2 \left| \tilde{G}_{12}^r(\varepsilon) \right|^2$ $[(\Gamma_2^L)^2 \left| \tilde{G}_{34}^r(\varepsilon) \right|^2]$ describes an electron with spin-up tunnelling from the left lead through quantum dot 1 (2) to the superconductor lead and reflecting a hole back to the left lead

through the quantum dot 1 (2). While the term $\Gamma_1^L \Gamma_2^L \left| \tilde{G}_{14}^r(\varepsilon) \right|^2 \left[\Gamma_1^L \Gamma_2^L \left| \tilde{G}_{32}^r(\varepsilon) \right|^2 \right]$ is for the spin-up electron tunneling from left lead through dot 1 (2) to the superconductor lead and a hole reflecting back to the left lead through the dot 2 (1). There exist other channels in which the tunnel electron and reflecting hole go through both two dots. The remaining part in Eq. (26) describes the interference effect of all possible multichannels of the device. The transmission probability from left to right leads reads

$$\begin{aligned}
T_{LR} = & \Gamma_1^L \left[\Gamma_1^R \left| \tilde{G}_{11}^r(\varepsilon) \right|^2 + \Gamma_1^R \left| \tilde{G}_{12}^r(\varepsilon) \right|^2 \right. \\
& + \Gamma_2^R \left| \tilde{G}_{13}^r(\varepsilon) \right|^2 + \Gamma_2^R \left| \tilde{G}_{14}^r(\varepsilon) \right|^2 \left. \right] \\
& + \Gamma_2^L \left[\Gamma_1^R \left| \tilde{G}_{31}^r(\varepsilon) \right|^2 + \Gamma_1^R \left| \tilde{G}_{32}^r(\varepsilon) \right|^2 \right. \\
& + \Gamma_2^R \left| \tilde{G}_{33}^r(\varepsilon) \right|^2 + \Gamma_2^R \left| \tilde{G}_{34}^r(\varepsilon) \right|^2 \left. \right] \\
& + 2 \operatorname{Re} \left[-\Gamma_1^L \Gamma_1^R e^{-i\frac{\Phi}{2}} \frac{\Delta}{|\varepsilon|} \tilde{G}_{11}^r(\varepsilon) \tilde{G}_{12}^{r*}(\varepsilon) + \dots \right].
\end{aligned} \tag{27}$$

containing many terms which are understood. We are mainly interested in the physics of the Andreev reflections. As a matter of fact only the Andreev reflection process contributes to the current (i. e., $J_T = 0$) at zero temperature, if $|eV| < \Delta$. In the following section, we analyze time evolution of the probability of the Andreev reflection T_{AR} and the Andreev reflection current J_A as well depending on dc bias voltage, gate voltage, magnetic flux, and interdot coupling strength.

III. NUMERICAL RESULTS

First of all we transform the coupled-QD system into an effective decoupled one with bonding and antibonding dressed states of the QD molecule using the following transformation [23],

$$\begin{pmatrix} f_+ \\ f_- \end{pmatrix} = \begin{pmatrix} -\cos \beta e^{i\Phi_{12}} & -\sin \beta \\ -\sin \beta & \cos \beta e^{-i\Phi_{12}} \end{pmatrix} \begin{pmatrix} d_1 \\ d_2 \end{pmatrix}. \tag{28}$$

where, f_- and f_+ are the annihilation operators of the bonding and antibonding dressed states for the QD molecule. And β is defined as $1/2 \tan^{-1}[2\Omega/(\varepsilon_1 - \varepsilon_2)]$. Thus the Hamiltonian for coupled double quantum dot H_D is diagonalized as

$$\tilde{H}_D = E_+ f_+^\dagger f_+ + E_- f_-^\dagger f_-, \tag{29}$$

where

$$E_\pm = \frac{1}{2} [\varepsilon_1 + \varepsilon_2 \pm \sqrt{(\varepsilon_1 - \varepsilon_2)^2 + 4\Omega^2}]. \tag{30}$$

Considering the tunneling Hamiltonian between double QD and the left lead, we obtain the linewidth Γ_+^L and Γ_-^L corresponding to the antibonding and bonding states coupled to the left lead, respectively, as

$$\Gamma_+^L = \Gamma_1^L \cos^2 \beta + \Gamma_2^L \sin^2 \beta + \sqrt{\Gamma_1^L \Gamma_2^L} \sin(2\beta) \cos\left(\frac{\Phi}{2} + \Phi_{12}\right), \tag{31}$$

$$\Gamma_-^L = \Gamma_1^L \sin^2 \beta + \Gamma_2^L \cos^2 \beta - \sqrt{\Gamma_1^L \Gamma_2^L} \sin(2\beta) \cos\left(\frac{\Phi}{2} + \Phi_{12}\right). \tag{32}$$

In the numerical analysis we set $\Delta = 1$ as the energy unit. The energy dependence of reflection probability T_{AR} on the interdot coupling strength is shown in Fig. 2 for the symmetry [with $\Gamma_1^L = \Gamma_1^R = \Gamma_2^L = \Gamma_2^R = 0.02$, Fig.2(a)] and asymmetry [with $\Gamma_1^L = \Gamma_2^L = 0.08$, $\Gamma_1^R = \Gamma_2^R = 0.02$, Fig.2(b) and $\Gamma_1^L = \Gamma_1^R = 0.08$, $\Gamma_2^L = \Gamma_2^R = 0.02$, Fig.2(c)] cases, respectively. Other parameters are chosen as $\varepsilon_1 = \varepsilon_2 = 0$, and $\Phi = \Phi_{12} = 0$. It is seen in Fig. 2(a) that if the two QDs are completely decoupled (i.e., $\Omega = 0$) only a single peak appears (solid line), and when $\Omega \neq 0$, two peaks emerges at $\varepsilon = \pm\Omega$ due to the existence of two energy levels. The maximum of peaks is getting lower when the coupling constant Ω is increasing. For the asymmetry case Fig. 2(b) shows that there are no significant two peaks. Fig. 2(c) exhibits the complex spectra due to the possible overlap of the broad levels similar to the interpretation of

Fano effect in a parallel coupled double QD connected to two normal metal leads system [23]. And when Ω is large enough such that the broad two energy levels are completely separated, the two single peaks remain at $\varepsilon = E_+$ and E_- .

It is interesting to see the effect of the magnetic flux on the Andreev reflection and Fig. 3 presents the dependence of the Andreev reflection probability on the magnetic flux Φ with $\alpha_1 = \alpha_2$ and therefore $\Phi_{12} = 0$. The height of peaks at $\varepsilon = \pm\Omega$ can reach 2 when the magnetic flux is nonzero, and magnetic flux also has an influence on the width of the peaks, i. e., on the linewidth function Γ_{\pm} , here we choose $\Phi = \pi/3$ for a solid line, and $2\pi/3$ for a dotted line, the height of peaks are not changed. Electron phase coherence is shown in Fig. 4. When $\Omega = 0$, i. e., there is no the interdot coupling, the oscillation period of the Andreev reflection probability vs magnetic flux is $2\pi\Phi_0$ (solid line), while $\Omega \neq 0$, the period changes to $4\pi\Phi_0$ when $\alpha_1 = \alpha_2$ [see Fig. 4(a)]. Here, we choose the different energy eigenvalues such that $\varepsilon = 0.11$, since at those values the probability of the Andreev reflection reaches maximum. To see the reason of the period changing, we give a general result of the oscillation period when $\alpha_1/\alpha_2 = n$. The channel paths contain two parts due to the Andreev reflection in the hybrid system. One is the incident electron from the left lead to the superconductor in Fig. 5a, the other is the reflecting hole from the superconductor to the left lead in Fig. 5b. The phase shift of electron in the case (3) in Fig. 5a is $(\Phi_1 - \Phi_2)/2$, and the corresponding phase shift of hole in the case (1) in Fig. 5b is $(\Phi_1 + \Phi_2)/2$, so the total shift of the channel (3) for the electron and (1) for the hole is Φ_1 . The interference effect corresponds to all the channel paths reads [25]

$$\begin{aligned}
T &= \left| \begin{array}{c} A_0 + A_1 e^{i\Phi_1} + A_2 e^{-i\Phi_1} + A_3 e^{i\Phi_2} + A_4 e^{-i\Phi_2} + A_5 e^{i(\Phi_1 + \Phi_2)} \\ + A_6 e^{-i(\Phi_1 + \Phi_2)} + A_7 e^{i(\Phi_1 - \Phi_2)} + A_8 e^{-i(\Phi_1 - \Phi_2)} \end{array} \right|^2 \\
&= B_0 + B_1 \cos \Phi_1 + B_2 \cos \Phi_2 + B_3 \cos(\Phi_1 + \Phi_2) \\
&\quad + B_4 \cos(\Phi_1 - \Phi_2) + B_5 \cos 2\Phi_1 + B_6 \cos 2\Phi_2 \\
&\quad + B_7 \cos 2(\Phi_1 + \Phi_2) + B_8 \cos(2\Phi_1 + \Phi_2) + B_9 \cos(\Phi_1 + 2\Phi_2) \\
&\quad + B_{10} \cos 2(\Phi_1 - \Phi_2) + B_{11} \cos(2\Phi_1 - \Phi_2) + B_{12} \cos(\Phi_1 - 2\Phi_2)
\end{aligned} \tag{33}$$

where parameters A are the amplitudes of channel paths. With $\Phi_1 = \Phi n/(n+1)$, $\Phi_2 = \Phi/(n+1)$, Eq. (33) shows the oscillation periods might have π , 2π , $2\pi(n+1)/n$, $2\pi(n+1)$, $2\pi(n+1)/2n$, $2\pi(n+1)/2$, $2\pi(n+1)/(n-1)$, $2\pi(n+1)/(n-2)$, $2\pi(n+1)/(n+2)$, $2\pi(n+1)/(2n+1)$, and $2\pi(n+1)/(2n-1)$, suggesting that the oscillation period of reflect probability should be $2(n+1)\pi$. The linear dependence of the ratio n is further confirmed in Fig. 4(b), it shows that the oscillation period is 6π for $n = 2$ (solid line), 8π for $n = 3$ (dotted line), and 10π for $n = 4$ (dashed line). The linear manner of the oscillation period is the same as the one in Ref. 22, however, the mechanism is different: there the transmitted current is analyzed.

Fig. 6 shows current-gate-voltage curve (J_A vs V_g) for the case that $\varepsilon_1 = 0.1$, $\varepsilon_2 = 0.3$, $\Phi = \Phi_{12} = 0$, and the bias voltage $V = 0.4$. We assume that the energy levels in both dots are connected to the same voltage through the capacitive coupling. When $\Omega = 0$ (solid line), there exist two smaller peaks at $V_g = 0.1$, and 0.3 located symmetrically beside the larger peak at $V_g = 0.2$ with the height that is two times higher than the height of the smaller peaks. The interpretation of the phenomena is similar to that in Ref. [15] such that when $V_g = 0.1$ the energy level ε_1 matches with chemical potential $u_R = 0$ in the right superconductor lead and the Andreev reflection takes place at this level. When $V_g = 0.2$ two energy levels have a symmetric localization about u_R (ε_2 is 0.1 above u_R while ε_1 is 0.1 below u_R) and both ε_1 and ε_2 are below the bias voltage, so the Andreev reflection that involves those two levels leads to the height of the peaks that are two times higher than that containing only one energy level. The interpretation is the same for the gate voltage $V_g = 0.3$ where the energy level ε_2 matches with u_R . Some new properties are observed for the coupled case $\Omega \neq 0$: (1) the location of the middle peak does not change, while the positions of the left and right peaks shift towards the left and right sides, respectively, with the increasing coupling strength Ω . (2) the heights of the left and the middle peaks are suppressed significantly; meantime, the height of the right peak is enhanced. (3) the widths of the left and middle peaks decrease while the width of the right peak widened. These interesting phenomena can be explained with Eq. (30)-(32). The energy level of dressed state E_+ gets larger and E_- becomes smaller with increasing coupling strength Ω , and at the end E_+ is higher than energy level of bared state ε_2 , when E_- is smaller than ε_1 . So when the gate voltage takes action on the dressed states, the left peak runs towards the left while the right peak goes opposite, however, the locations of the two peaks remain symmetric about the middle peak. We assume $E_- = \varepsilon_1 - a = 0.1 - a$, $E_+ = \varepsilon_2 + a = 0.3 + a$, where a is introduced due to the coupling strength Ω . So when the gate voltage becomes $V_g = 0.1 - a$, the left peak emerges and with increasing V_g (up to 0.2), both two dressed states levels locate symmetrically about u_R . Thus, the location of middle peak does not change at $V_g = 0.2$, no matter how the parameter $a(\Omega)$ varies. The linewidth of dressed states, Γ_{\pm}^L , increases with the increasing of Ω , while Γ_{\pm}^R decreases under the parameters considered here, and hence, the right peak gets wider and left peak becomes narrower with the increasing of Ω . The linewidths Γ_{\pm} are directly connected with the coupling strengths between

QD and the leads. The widening of the right-side peak means the increasing of coupling strength between dressed state E_+ and the leads. Therefore, the height of the right-side peak is enhanced, and opposite to this, the height of the left-side peak is suppressed. The suppression of the middle-peak height suggests that the Andreev resonance involving two energy levels gets maximum when two energy levels are symmetric.

Figures. 7 – 9 show a tunable Andreev reflection current depending on the magnetic flux when $\Omega \neq 0$. In Fig. 7, we fix $\Phi = \pi/2$, and tune the value of Φ_{12} for different curves. One can see that the height of the right peak is enhanced and the height of the left one is suppressed while the height of the middle peak does not change with the increase of Φ_{12} . It is interesting to notice that the left peaks has essentially no changes when $\Phi_{12} = 0$ (solid line) and $\pi/2$ (dotted line), while the right peak changes conspicuously with respect to the case without the magnetic flux. Figure 8 has the opposite effect compared with Fig. 7, namely, the height of the left peak is suppressed while the height of the right one is enhanced and the middle peak does not vary with Φ_{12} . We fix $\Phi_{12} = \pi/5$, and vary values of magnetic flux Φ in Fig. 9, it is shown that the height of three peaks can be tuned simultaneously.

IV. CONCLUSIONS

We have studied the tunable Andreev reflection in a double AB interferometer in terms of the nonequilibrium Green function method and observed several features of the reflection current. It is found that the oscillation period of the Andreev reflection probability with the magnetic flux is 2π when interdot coupling vanishes ($\Omega = 0$, in this case the system reduces to a single interferometer), while it is $2(n+1)\pi$ for our double interferometer ($\Omega \neq 0$) where n is the ratio of two parts magnetic fluxes, i.e. $n = \Phi_1/\Phi_2$. The Andreev reflection current peaks cannot only be tuned by coupling strength Ω , but also by magnetic flux.

V. ACKNOWLEDGMENT

This work was supported by the National Natural Science Foundation of China under Grant No. 10475053

VI. APPENDIX A

In this appendix, we present the derivation of the Green function of Eq. (18) in detail. From Eqs. (8)-(13) and (17) we have the following formulas for the matrix elements of Green function $G^r(t, t')$ in the energy representation:

$$\begin{aligned} g_{11}^{r-1}(E')G_{11}^r(E, E') &= 2\pi\delta(E - E') - A_1G_{11}^r(E, E') \\ &\quad + B\Gamma_1^R e^{i\frac{\Phi}{2}} G_{12}^r(E, E') + x_1G_{13}^r(E, E') \\ &\quad + B\sqrt{\Gamma_1^R\Gamma_2^R} G_{14}^r(E, E'), \end{aligned} \quad (\text{A1})$$

$$\begin{aligned} g_{22}^{r-1}(E')G_{12}^r(E, E') &= B\Gamma_1^R e^{-i\frac{\Phi}{2}} G_{11}^r(E, E') - A_1G_{12}^r(E, E') \\ &\quad + B\sqrt{\Gamma_1^R\Gamma_2^R} G_{13}^r(E, E') + x_2G_{14}^r(E, E'), \end{aligned} \quad (\text{A2})$$

$$\begin{aligned} g_{33}^{r-1}(E')G_{13}^r(E, E') &= x_3G_{11}^r(E, E') + B\sqrt{\Gamma_1^R\Gamma_2^R} G_{12}^r(E, E') \\ &\quad - A_2G_{13}^r(E, E') + B\Gamma_2^R e^{-i\frac{\Phi}{2}} G_{14}^r(E, E'), \end{aligned} \quad (\text{A3})$$

$$\begin{aligned} g_{44}^{r-1}(E')G_{14}^r(E, E') &= B\sqrt{\Gamma_1^R\Gamma_2^R} G_{11}^r(E, E') + x_1G_{12}^r(E, E') \\ &\quad + B\Gamma_2^R e^{i\frac{\Phi}{2}} G_{13}^r(E, E') - A_2G_{14}^r(E, E'), \end{aligned} \quad (\text{A4})$$

where

$$\begin{aligned}
A_1 &= \frac{i}{2}(\Gamma_1^L + \Gamma_1^R \frac{|E'|}{\sqrt{(E')^2 - \Delta^2}}), \\
A_2 &= \frac{i}{2}(\Gamma_2^L + \Gamma_2^R \frac{|E'|}{\sqrt{(E')^2 - \Delta^2}}), \\
B &= \frac{i}{2} \frac{\Delta}{\sqrt{(E')^2 - \Delta^2}},
\end{aligned} \tag{A5}$$

and

$$\begin{aligned}
x_1 &= \Omega e^{i\Phi_{12}} - \frac{i}{2} \sqrt{\Gamma_1^L \Gamma_2^L} e^{-i\frac{\Phi}{2}} - \frac{i}{2} \frac{|E'|}{\sqrt{(E')^2 - \Delta^2}} \sqrt{\Gamma_1^R \Gamma_2^R} e^{i\frac{\Phi}{2}}, \\
x_2 &= -\Omega^* e^{-i\Phi_{12}} - \frac{i}{2} \sqrt{\Gamma_1^L \Gamma_2^L} e^{i\frac{\Phi}{2}} - \frac{i}{2} \frac{|E'|}{\sqrt{(E')^2 - \Delta^2}} \sqrt{\Gamma_1^R \Gamma_2^R} e^{-i\frac{\Phi}{2}}, \\
x_3 &= \Omega^* e^{-i\Phi_{12}} - \frac{i}{2} \sqrt{\Gamma_1^L \Gamma_2^L} e^{i\frac{\Phi}{2}} - \frac{i}{2} \frac{|E'|}{\sqrt{(E')^2 - \Delta^2}} \sqrt{\Gamma_1^R \Gamma_2^R} e^{-i\frac{\Phi}{2}}, \\
x_4 &= -\Omega e^{i\Phi_{12}} - \frac{i}{2} \sqrt{\Gamma_1^L \Gamma_2^L} e^{-i\frac{\Phi}{2}} - \frac{i}{2} \frac{|E'|}{\sqrt{(E')^2 - \Delta^2}} \sqrt{\Gamma_1^R \Gamma_2^R} e^{i\frac{\Phi}{2}}.
\end{aligned} \tag{A6}$$

Solving those coupled equations, the results are obtained as

$$\begin{aligned}
G_{11}^r(E, E') &= 2\pi \tilde{G}_{11}^r(E') \delta(E - E'), \\
G_{12}^r(E, E') &= 2\pi \tilde{G}_{12}^r(E') \delta(E - E'), \\
G_{13}^r(E, E') &= 2\pi \tilde{G}_{13}^r(E') \delta(E - E'), \\
G_{14}^r(E, E') &= 2\pi \tilde{G}_{14}^r(E') \delta(E - E'),
\end{aligned} \tag{A7}$$

where

$$\tilde{G}_{11}^r(E') = \frac{1}{M(E')} \begin{vmatrix} g_{22}^{r-1}(E') + A_1 & -B\sqrt{\Gamma_1^R \Gamma_2^R} & -x_2 \\ -B\sqrt{\Gamma_1^R \Gamma_2^R} & g_{33}^{r-1}(E') + A_2 & -B\Gamma_2^R e^{-i\frac{\Phi}{2}} \\ -x_4 & -B\Gamma_2^R e^{i\frac{\Phi}{2}} & g_{44}^{r-1}(E') + A_2 \end{vmatrix}, \tag{A8}$$

$$\tilde{G}_{12}^r(E') = -\frac{1}{M(E')} \begin{vmatrix} -B\Gamma_1^R e^{-i\frac{\Phi}{2}} & -B\sqrt{\Gamma_1^R \Gamma_2^R} & -x_2 \\ -x_3 & g_{33}^{r-1}(E') + A_2 & -B\Gamma_2^R e^{-i\frac{\Phi}{2}} \\ -B\sqrt{\Gamma_1^R \Gamma_2^R} & -B\Gamma_2^R e^{i\frac{\Phi}{2}} & g_{44}^{r-1}(E') + A_2 \end{vmatrix}, \tag{A9}$$

$$\tilde{G}_{13}^r(E') = \frac{1}{M(E')} \begin{vmatrix} -B\Gamma_1^R e^{-i\frac{\Phi}{2}} & g_{22}^{r-1}(E') + A_1 & -x_2 \\ -x_3 & -B\sqrt{\Gamma_1^R \Gamma_2^R} & -B\Gamma_2^R e^{-i\frac{\Phi}{2}} \\ -B\sqrt{\Gamma_1^R \Gamma_2^R} & -x_4 & g_{44}^{r-1}(E') + A_2 \end{vmatrix}, \tag{A10}$$

$$\tilde{G}_{14}^r(E') = -\frac{1}{M(E')} \begin{vmatrix} -B\Gamma_1^R e^{-i\frac{\Phi}{2}} & g_{22}^{r-1}(E') + A_1 & -B\sqrt{\Gamma_1^R \Gamma_2^R} \\ -x_3 & -B\sqrt{\Gamma_1^R \Gamma_2^R} & g_{33}^{r-1}(E') + A_2 \\ -B\sqrt{\Gamma_1^R \Gamma_2^R} & -x_4 & -B\Gamma_2^R e^{i\frac{\Phi}{2}} \end{vmatrix}, \tag{A11}$$

here,

$$M(E') = \begin{vmatrix} g_{11}^{r-1}(E') + A_1 & -B\Gamma_1^R e^{i\frac{\Phi}{2}} & -x_1 & -B\sqrt{\Gamma_1^R \Gamma_2^R} \\ -B\Gamma_1^R e^{-i\frac{\Phi}{2}} & g_{22}^{r-1}(E') + A_1 & -B\sqrt{\Gamma_1^R \Gamma_2^R} & -x_2 \\ -x_3 & -B\sqrt{\Gamma_1^R \Gamma_2^R} & g_{33}^{r-1}(E') + A_2 & -B\Gamma_2^R e^{-i\frac{\Phi}{2}} \\ -B\sqrt{\Gamma_1^R \Gamma_2^R} & -x_4 & -B\Gamma_2^R e^{i\frac{\Phi}{2}} & g_{44}^{r-1}(E') + A_2 \end{vmatrix}. \tag{A12}$$

With the same procedure we have

$$\begin{aligned}
g_{11}^{r-1}(E')G_{31}^r(E, E') &= -A_1G_{31}^r(E, E') + B\Gamma_1^R e^{i\frac{\Phi}{2}}G_{32}^r(E, E') \\
&\quad + x_1G_{33}^r(E, E') + B\sqrt{\Gamma_1^R\Gamma_2^R}G_{34}^r(E, E'),
\end{aligned} \tag{A13}$$

$$\begin{aligned}
g_{22}^{r-1}(E')G_{32}^r(E, E') &= B\Gamma_1^R e^{-i\frac{\Phi}{2}}G_{31}^r(E, E') - A_1G_{32}^r(E, E') \\
&\quad + B\sqrt{\Gamma_1^R\Gamma_2^R}G_{33}^r(E, E') + x_2G_{34}^r(E, E'),
\end{aligned} \tag{A14}$$

$$\begin{aligned}
g_{33}^{r-1}(E')G_{33}^r(E, E') &= 2\pi\delta(E - E') + x_3G_{31}^r(E, E') \\
&\quad + B\sqrt{\Gamma_1^R\Gamma_2^R}G_{32}^r(E, E') - A_2G_{33}^r(E, E') \\
&\quad + B\Gamma_2^R e^{-i\frac{\Phi}{2}}G_{34}^r(E, E'),
\end{aligned} \tag{A15}$$

$$\begin{aligned}
g_{44}^{r-1}(E')G_{34}^r(E, E') &= B\sqrt{\Gamma_1^R\Gamma_2^R}G_{31}^r(E, E') + x_4G_{32}^r(E, E') \\
&\quad + B\Gamma_2^R e^{i\frac{\Phi}{2}}G_{33}^r(E, E') - A_2G_{44}^r(E, E').
\end{aligned} \tag{A16}$$

So the final results are

$$\begin{aligned}
G_{31}^r(E, E') &= 2\pi\tilde{G}_{31}^r(E')\delta(E - E') \\
G_{32}^r(E, E') &= 2\pi\tilde{G}_{32}^r(E')\delta(E - E') \\
G_{33}^r(E, E') &= 2\pi\tilde{G}_{33}^r(E')\delta(E - E') \\
G_{34}^r(E, E') &= 2\pi\tilde{G}_{34}^r(E')\delta(E - E')
\end{aligned} \tag{A17}$$

where

$$\tilde{G}_{31}^r(E') = \frac{1}{M(E')} \begin{vmatrix} -B\Gamma_1^R e^{i\frac{\Phi}{2}} & -x_1 & -B\sqrt{\Gamma_1^R\Gamma_2^R} \\ g_{22}^{r-1}(E') + A_1 & -B\sqrt{\Gamma_1^R\Gamma_2^R} & -x_2 \\ -x_4 & -B\Gamma_2^R e^{i\frac{\Phi}{2}} & g_{44}^{r-1}(E') + A_2 \end{vmatrix} \tag{A18}$$

$$\tilde{G}_{32}^r(E') = -\frac{1}{M(E')} \begin{vmatrix} g_{11}^{r-1}(E') + A_1 & -x_1 & -B\sqrt{\Gamma_1^R\Gamma_2^R} \\ -B\Gamma_1^R e^{-i\frac{\Phi}{2}} & -B\sqrt{\Gamma_1^R\Gamma_2^R} & -x_2 \\ -B\sqrt{\Gamma_1^R\Gamma_2^R} & -B\Gamma_2^R e^{i\frac{\Phi}{2}} & g_{44}^{r-1}(E') + A_2 \end{vmatrix} \tag{A19}$$

$$\tilde{G}_{33}^r(E') = \frac{1}{M(E')} \begin{vmatrix} g_{11}^{r-1}(E') + A_1 & -B\Gamma_1^R e^{i\frac{\Phi}{2}} & -B\sqrt{\Gamma_1^R\Gamma_2^R} \\ -B\Gamma_1^R e^{-i\frac{\Phi}{2}} & g_{22}^{r-1}(E') + A_1 & -x_2 \\ -B\sqrt{\Gamma_1^R\Gamma_2^R} & -x_4 & g_{44}^{r-1}(E') + A_2 \end{vmatrix} \tag{A20}$$

$$\tilde{G}_{34}^r(E') = -\frac{1}{M(E')} \begin{vmatrix} g_{11}^{r-1}(E') + A_1 & -B\Gamma_1^R e^{i\frac{\Phi}{2}} & -x_1 \\ -B\Gamma_1^R e^{-i\frac{\Phi}{2}} & g_{22}^{r-1}(E') + A_1 & -B\sqrt{\Gamma_1^R\Gamma_2^R} \\ -B\sqrt{\Gamma_1^R\Gamma_2^R} & -x_4 & -B\Gamma_2^R e^{i\frac{\Phi}{2}} \end{vmatrix} \tag{A21}$$

VII. APPENDIX B

The complete expression of matrix elements of the Green function $G^<(t, t)$ is

$$\begin{aligned}
G_{11}^{\leq}(t, t) = & i \int \frac{d\varepsilon}{2\pi} \{ f_L(\varepsilon + eV) \Gamma_1^L \left| \tilde{G}_{11}^r(\varepsilon) \right|^2 + f_L(\varepsilon - eV) \Gamma_1^L \left| \tilde{G}_{12}^r(\varepsilon) \right|^2 \\
& + f_L(\varepsilon + eV) \Gamma_2^L \left| \tilde{G}_{13}^r(\varepsilon) \right|^2 + f_L(\varepsilon - eV) \Gamma_2^L \left| \tilde{G}_{14}^r(\varepsilon) \right|^2 \\
& + 2\sqrt{\Gamma_1^L \Gamma_2^L} \operatorname{Re}[f_L(\varepsilon + eV) e^{i\frac{\Phi}{2}} \tilde{G}_{11}^r(\varepsilon) \tilde{G}_{13}^{r*}(\varepsilon) \\
& + f_L(\varepsilon - eV) e^{-i\frac{\Phi}{2}} \tilde{G}_{12}^r(\varepsilon) \tilde{G}_{14}^{r*}(\varepsilon)] \} \\
& + i \int \frac{d\varepsilon}{2\pi} f_R(\varepsilon) \tilde{\rho}_R(\varepsilon) \{ \Gamma_1^R \left| \tilde{G}_{11}^r(\varepsilon) \right|^2 + \Gamma_1^R \left| \tilde{G}_{12}^r(\varepsilon) \right|^2 \\
& + \Gamma_2^R \left| \tilde{G}_{13}^r(\varepsilon) \right|^2 + \Gamma_2^R \left| \tilde{G}_{14}^r(\varepsilon) \right|^2 \\
& + 2 \operatorname{Re}[-\Gamma_1^R e^{-i\frac{\Phi}{2}} \frac{\Delta}{|\varepsilon|} \tilde{G}_{11}^r(\varepsilon) \tilde{G}_{12}^{r*}(\varepsilon) \\
& + \sqrt{\Gamma_1^R \Gamma_2^R} e^{-i\frac{\Phi}{2}} \tilde{G}_{11}^r(\varepsilon) \tilde{G}_{13}^{r*}(\varepsilon) + \sqrt{\Gamma_1^R \Gamma_2^R} e^{i\frac{\Phi}{2}} \tilde{G}_{12}^r(\varepsilon) \tilde{G}_{14}^{r*}(\varepsilon) \\
& - \Gamma_2^R e^{i\frac{\Phi}{2}} \frac{\Delta}{|\varepsilon|} \tilde{G}_{13}^r(\varepsilon) \tilde{G}_{14}^{r*}(\varepsilon) - \sqrt{\Gamma_1^R \Gamma_2^R} \frac{\Delta}{|\varepsilon|} \tilde{G}_{11}^r(\varepsilon) \tilde{G}_{14}^{r*}(\varepsilon) \\
& - \sqrt{\Gamma_1^R \Gamma_2^R} \frac{\Delta}{|\varepsilon|} \tilde{G}_{12}^r(\varepsilon) \tilde{G}_{13}^{r*}(\varepsilon)] \}, \tag{B1}
\end{aligned}$$

$$\begin{aligned}
G_{13}^{\leq}(t, t) = & i \int \frac{d\varepsilon}{2\pi} [f_L(\varepsilon + eV) \Gamma_1^L \tilde{G}_{11}^r(\varepsilon) \tilde{G}_{13}^a(\varepsilon) + f_L(\varepsilon + eV) \sqrt{\Gamma_1^L \Gamma_2^L} e^{-i\frac{\Phi}{2}} \tilde{G}_{13}^r(\varepsilon) \tilde{G}_{13}^a(\varepsilon) \\
& + f_L(\varepsilon - eV) \Gamma_1^L \tilde{G}_{12}^r(\varepsilon) \tilde{G}_{23}^a(\varepsilon) + f_L(\varepsilon - eV) \sqrt{\Gamma_1^L \Gamma_2^L} e^{i\frac{\Phi}{2}} \tilde{G}_{14}^r(\varepsilon) \tilde{G}_{23}^a(\varepsilon) \\
& + f_L(\varepsilon + eV) \sqrt{\Gamma_1^L \Gamma_2^L} e^{i\frac{\Phi}{2}} \tilde{G}_{11}^r(\varepsilon) \tilde{G}_{33}^a(\varepsilon) + f_L(\varepsilon + eV) \Gamma_2^L \tilde{G}_{13}^r(\varepsilon) \tilde{G}_{33}^a(\varepsilon) \\
& + f_L(\varepsilon - eV) \sqrt{\Gamma_1^L \Gamma_2^L} e^{-i\frac{\Phi}{2}} \tilde{G}_{12}^r(\varepsilon) \tilde{G}_{43}^a(\varepsilon) + f_L(\varepsilon - eV) \Gamma_2^L \tilde{G}_{14}^r(\varepsilon) \tilde{G}_{43}^a(\varepsilon)] \\
& + i \int \frac{d\varepsilon}{2\pi} f_R(\varepsilon) \tilde{\rho}_R(\varepsilon) \{ [\Gamma_1^R \tilde{G}_{11}^r(\varepsilon) - \Gamma_1^R e^{i\frac{\Phi}{2}} \frac{\Delta}{|\varepsilon|} \tilde{G}_{12}^r(\varepsilon) + \sqrt{\Gamma_1^R \Gamma_2^R} e^{i\frac{\Phi}{2}} \tilde{G}_{13}^r(\varepsilon) \\
& - \sqrt{\Gamma_1^R \Gamma_2^R} \frac{\Delta}{|\varepsilon|} \tilde{G}_{14}^r(\varepsilon)] \tilde{G}_{13}^a(\varepsilon) + [-\Gamma_1^R e^{-i\frac{\Phi}{2}} \frac{\Delta}{|\varepsilon|} \tilde{G}_{11}^r(\varepsilon) + \Gamma_1^R \tilde{G}_{12}^r(\varepsilon) \\
& - \sqrt{\Gamma_1^R \Gamma_2^R} \frac{\Delta}{|\varepsilon|} \tilde{G}_{13}^r(\varepsilon) + \sqrt{\Gamma_1^R \Gamma_2^R} e^{-i\frac{\Phi}{2}} \tilde{G}_{14}^r(\varepsilon)] \tilde{G}_{23}^a(\varepsilon) \\
& + [\sqrt{\Gamma_1^R \Gamma_2^R} e^{-i\frac{\Phi}{2}} \tilde{G}_{11}^r(\varepsilon) - \sqrt{\Gamma_1^R \Gamma_2^R} \frac{\Delta}{|\varepsilon|} \tilde{G}_{12}^r(\varepsilon) + \Gamma_2^R \tilde{G}_{13}^r(\varepsilon) \\
& - \Gamma_2^R e^{-i\frac{\Phi}{2}} \frac{\Delta}{|\varepsilon|} \tilde{G}_{14}^r(\varepsilon)] \tilde{G}_{33}^a(\varepsilon) + [-\sqrt{\Gamma_1^R \Gamma_2^R} \frac{\Delta}{|\varepsilon|} \tilde{G}_{11}^r(\varepsilon) \\
& + \sqrt{\Gamma_1^R \Gamma_2^R} e^{i\frac{\Phi}{2}} \tilde{G}_{12}^r(\varepsilon) - \Gamma_2^R e^{i\frac{\Phi}{2}} \frac{\Delta}{|\varepsilon|} \tilde{G}_{13}^r(\varepsilon) + \Gamma_2^R \tilde{G}_{14}^r(\varepsilon)] \tilde{G}_{43}^a(\varepsilon) \}, \tag{B2}
\end{aligned}$$

$$\begin{aligned}
G_{31}^{\leq}(t, t) = & i \int \frac{d\varepsilon}{2\pi} [f_L(\varepsilon + eV) \Gamma_1^L \tilde{G}_{31}^r(\varepsilon) \tilde{G}_{11}^a(\varepsilon) + f_L(\varepsilon + eV) \sqrt{\Gamma_1^L \Gamma_2^L} e^{-i\frac{\Phi}{2}} \tilde{G}_{33}^r(\varepsilon) \tilde{G}_{11}^a(\varepsilon) \\
& + f_L(\varepsilon - eV) \Gamma_1^L \tilde{G}_{32}^r(\varepsilon) \tilde{G}_{21}^a(\varepsilon) + f_L(\varepsilon - eV) \sqrt{\Gamma_1^L \Gamma_2^L} e^{i\frac{\Phi}{2}} \tilde{G}_{34}^r(\varepsilon) \tilde{G}_{21}^a(\varepsilon) \\
& + f_L(\varepsilon + eV) \sqrt{\Gamma_1^L \Gamma_2^L} e^{i\frac{\Phi}{2}} \tilde{G}_{31}^r(\varepsilon) \tilde{G}_{31}^a(\varepsilon) + f_L(\varepsilon + eV) \Gamma_2^L \tilde{G}_{33}^r(\varepsilon) \tilde{G}_{31}^a(\varepsilon) \\
& + f_L(\varepsilon - eV) \sqrt{\Gamma_1^L \Gamma_2^L} e^{-i\frac{\Phi}{2}} \tilde{G}_{32}^r(\varepsilon) \tilde{G}_{41}^a(\varepsilon) + f_L(\varepsilon - eV) \Gamma_2^L \tilde{G}_{34}^r(\varepsilon) \tilde{G}_{41}^a(\varepsilon)] \\
& + i \int \frac{d\varepsilon}{2\pi} f_R(\varepsilon) \tilde{\rho}_R(\varepsilon) \{ [\Gamma_1^R \tilde{G}_{31}^r(\varepsilon) - \Gamma_1^R e^{i\frac{\Phi}{2}} \frac{\Delta}{|\varepsilon|} \tilde{G}_{32}^r(\varepsilon) + \sqrt{\Gamma_1^R \Gamma_2^R} e^{i\frac{\Phi}{2}} \tilde{G}_{33}^r(\varepsilon) \\
& - \sqrt{\Gamma_1^R \Gamma_2^R} \frac{\Delta}{|\varepsilon|} \tilde{G}_{34}^r(\varepsilon)] \tilde{G}_{11}^a(\varepsilon) + [-\Gamma_1^R e^{-i\frac{\Phi}{2}} \frac{\Delta}{|\varepsilon|} \tilde{G}_{31}^r(\varepsilon) + \Gamma_1^R \tilde{G}_{32}^r(\varepsilon) \\
& + \sqrt{\Gamma_1^R \Gamma_2^R} e^{-i\frac{\Phi}{2}} \tilde{G}_{33}^r(\varepsilon) - \sqrt{\Gamma_1^R \Gamma_2^R} \frac{\Delta}{|\varepsilon|} \tilde{G}_{34}^r(\varepsilon)] \tilde{G}_{21}^a(\varepsilon) + [\sqrt{\Gamma_1^R \Gamma_2^R} e^{i\frac{\Phi}{2}} \tilde{G}_{31}^r(\varepsilon) \\
& - \sqrt{\Gamma_1^R \Gamma_2^R} \frac{\Delta}{|\varepsilon|} \tilde{G}_{32}^r(\varepsilon) + \Gamma_2^R \tilde{G}_{33}^r(\varepsilon) - \Gamma_2^R e^{i\frac{\Phi}{2}} \frac{\Delta}{|\varepsilon|} \tilde{G}_{34}^r(\varepsilon)] \tilde{G}_{31}^a(\varepsilon) \\
& + [-\sqrt{\Gamma_1^R \Gamma_2^R} \frac{\Delta}{|\varepsilon|} \tilde{G}_{31}^r(\varepsilon) + \sqrt{\Gamma_1^R \Gamma_2^R} e^{-i\frac{\Phi}{2}} \tilde{G}_{32}^r(\varepsilon) - \Gamma_2^R e^{-i\frac{\Phi}{2}} \frac{\Delta}{|\varepsilon|} \tilde{G}_{33}^r(\varepsilon) \\
& + \Gamma_2^R \tilde{G}_{34}^r(\varepsilon)] \tilde{G}_{41}^a(\varepsilon) \}, \tag{B3}
\end{aligned}$$

$$\begin{aligned}
& -\sqrt{\Gamma_1^R \Gamma_2^R} \frac{\Delta}{|\varepsilon|} \tilde{G}_{33}(\varepsilon) + \sqrt{\Gamma_1^R \Gamma_2^R} e^{-i\frac{\Phi}{2}} \tilde{G}_{34}^r(\varepsilon) \tilde{G}_{21}^a(\varepsilon) \\
& + [\sqrt{\Gamma_1^R \Gamma_2^R} e^{-i\frac{\Phi}{2}} \tilde{G}_{31}^r(\varepsilon) - \sqrt{\Gamma_1^R \Gamma_2^R} \frac{\Delta}{|\varepsilon|} \tilde{G}_{32}^r(\varepsilon) + \Gamma_2^R \tilde{G}_{33}^r(\varepsilon) \\
& - \Gamma_2^R e^{-i\frac{\Phi}{2}} \frac{\Delta}{|\varepsilon|} \tilde{G}_{34}^r(\varepsilon)] \tilde{G}_{31}^a(\varepsilon) + [-\sqrt{\Gamma_1^R \Gamma_2^R} \frac{\Delta}{|\varepsilon|} \tilde{G}_{31}^r(\varepsilon) \\
& + \sqrt{\Gamma_1^R \Gamma_2^R} e^{i\frac{\Phi}{2}} \tilde{G}_{32}^r(\varepsilon) - \Gamma_2^R e^{i\frac{\Phi}{2}} \frac{\Delta}{|\varepsilon|} \tilde{G}_{33}^r(\varepsilon) + \Gamma_2^R \tilde{G}_{34}^r(\varepsilon)] \tilde{G}_{41}^a(\varepsilon)\}, \\
G_{33}^<(t, t) = & i \int \frac{d\varepsilon}{2\pi} \{f_L(\varepsilon + eV) \Gamma_1^L |\tilde{G}_{31}^r(\varepsilon)|^2 + f_L(\varepsilon - eV) \Gamma_1^L |\tilde{G}_{32}^r(\varepsilon)|^2 \\
& + f_L(\varepsilon + eV) \Gamma_2^L |\tilde{G}_{33}^r(\varepsilon)|^2 + f_L(\varepsilon - eV) \Gamma_2^L |\tilde{G}_{34}^r(\varepsilon)|^2 \\
& + 2\sqrt{\Gamma_1^L \Gamma_2^L} \text{Re}[f_L(\varepsilon + eV) e^{i\frac{\Phi}{2}} \tilde{G}_{31}^r(\varepsilon) \tilde{G}_{33}^{r*}(\varepsilon) \\
& + f_L(\varepsilon - eV) e^{-i\frac{\Phi}{2}} \tilde{G}_{32}^r(\varepsilon) \tilde{G}_{34}^{r*}(\varepsilon)]\} \\
& + i \int \frac{d\varepsilon}{2\pi} f_R(\varepsilon) \tilde{\rho}_R(\varepsilon) \{\Gamma_1^R |\tilde{G}_{31}^r(\varepsilon)|^2 + \Gamma_1^R |\tilde{G}_{32}^r(\varepsilon)|^2 \\
& + \Gamma_2^R |\tilde{G}_{33}^r(\varepsilon)|^2 + \Gamma_2^R |\tilde{G}_{34}^r(\varepsilon)|^2 \\
& + 2 \text{Re}[-\Gamma_1^R e^{i\frac{\Phi}{2}} \frac{\Delta}{|\varepsilon|} \tilde{G}_{32}^r(\varepsilon) \tilde{G}_{31}^{r*}(\varepsilon) + \sqrt{\Gamma_1^R \Gamma_2^R} e^{i\frac{\Phi}{2}} \tilde{G}_{33}^r(\varepsilon) \tilde{G}_{31}^{r*}(\varepsilon) \\
& + \sqrt{\Gamma_1^R \Gamma_2^R} e^{i\frac{\Phi}{2}} \tilde{G}_{32}^r(\varepsilon) \tilde{G}_{34}^{r*}(\varepsilon) - \Gamma_2^R e^{i\frac{\Phi}{2}} \frac{\Delta}{|\varepsilon|} \tilde{G}_{33}^r(\varepsilon) \tilde{G}_{34}^{r*}(\varepsilon) \\
& - \sqrt{\Gamma_1^R \Gamma_2^R} \frac{\Delta}{|\varepsilon|} \tilde{G}_{32}^r(\varepsilon) \tilde{G}_{33}^{r*}(\varepsilon) - \sqrt{\Gamma_1^R \Gamma_2^R} \frac{\Delta}{|\varepsilon|} \tilde{G}_{31}^r(\varepsilon) \tilde{G}_{34}^{r*}(\varepsilon)]\}. \tag{B4}
\end{aligned}$$

The results here show that the above matrix elements of $G^<(t, t)$ do not depend on time t , because for the N-QD-S hybrid system, the current should be independent of time for the dc bias [15].

-
- [1] R. Schuster, E. Buks, M. Heiblum, D. Mahalu, V. Umansky, and H. Shtrikman, *Nature (London)* 385,417 (1997); Y. Ji, M. Heiblum, D. Sprinzak, D. Mahalu, H. Shtrikman, *Science* 290, 779 (2000).
 - [2] D. Goldhaber-Gordon et al., *Nature (London)* 391, 156 (1998).
 - [3] J. Göres, D. Goldhaber-Gordon, S. Heemeyer, M. A. Kastner, H. Shtrikman, D. Mahalu, and U. Meirav, *Phys. Rev. B* 62, 2188 (2000).
 - [4] Y. Meir, N. S. Wingreen, P. A. Lee, *Phys. Rev. Lett.* 70, 2601 (1993); N. Sergueev, Qing-feng Sun, H. Guo, B. G. Wang, and Jian Wang, *Phys. Rev. B* 65, 165303 (2002).
 - [5] P. Zhang, Q.-K. Xue, Y. P. Wang, and X. C. Xie, *Phys. Rev. Lett.* 89, 286803 (2002).
 - [6] Baigeng Wang, J. Wang, H. Guo, *Phys. Rev. B* 67, 092408 (2003); Y.-P. Zhang, J.-Q. Liang, *Phys. Lett. A* 329, 55 (2004).
 - [7] J.-X. Zhu and A. V. Balatsky, *Phys. Rev. B* 67, 165326 (2003); Zuo-zi Chen, Rong Lü, and Bang-fen Zhu, *Phys. Rev. B* 71, 165324 (2005).
 - [8] N. S. Wingreen, A.-P. Jauho and Y. Meir, *Phys. Rev. B* 48, R8487 (1993); A.-P. Jauho, N. S. Wingreen, and Y. Meir, *Phys. Rev. B* 50, 5528 (1994).
 - [9] C. A. Stafford, and N. S. Wingreen, *Phys. Rev. Lett.* 76, 1916 (1996); Chi-keung Lui, Baigeng Wang, and Jian Wang, *Phys. Rev. B* 70, 205316 (2004); Mou Yang, and Shu-Shen Li, *Phys. Rev. B* 70, 045318 (2004).
 - [10] S. A. Gurvitz, and Ya. S. Prager, *Phys. Rev. B* 53, 15932 (1996); Bing Dong, H. L. Cui, and X. L. Lei, *Phys. Rev. B* 69, 035324 (2004); Xin-Qi Li, Wen-Kai Zhang, Ping Cui, Jinshu Shao, Zhongshui Ma, and Y. J. Yan, *Phys. Rev. B* 69, 085315 (2004); T. M. Stace, and S. D. Barrett, *Phys. Rev. Lett.* 92, 136802 (2004).
 - [11] C. W. J. Beenakker, *Phys. Rev. B* 44, 1646 (1991).
 - [12] Zhen-Gang Zhu, Gang Su, Qing-Rong Zheng and Biao Jin, *Phys. Rev. B* 70, 174403 (2004).
 - [13] C. W. J. Beenakker, *Phys. Rev. B* 46, R12841 (1992).

- [14] N. R. Claughton, M. Leadbeater, and C. J. Lambert, *J. Phys.: Condens. Matter* 7, 8757 (1995).
[15] Qing-feng Sun, Jian Wang, and Tsung-han Lin, *Phys. Rev. B* 59, 3831 (1999).
[16] Qing-feng Sun, Jian Wang, and Tsung-han Lin, *Phys. Rev. B* 59, 13126 (1999).
[17] Yu Zhu, Tsung-han Lin, and Qing-feng Sun, *Phys. Rev. B* 69, 121302(R) (2004).
[18] Yu Zhu, Qing-feng Sun, and Tsung-han Lin, *Phys. Rev. B* 65, 024516 (2001).
[19] Jin-Fu Feng, and Shi-Jie Xiong, *Phys. Rev. B* 67, 045316 (2003).
[20] Xiufeng Cao, Yaoming Shi, Xiaolong Song, and Shiping Zhou, *Phys. Rev. B* 70, 235341 (2004).
[21] E. Buks, R. Schuster, M. Heiblum, D. Mahalu, and V. Umansky, *Nature (London)* 391,871 (1998).
[22] Z. T. Jiang, J. Q. You, S. B. Bain, and H. Z. Zheng, *Phys. Rev. B* 66, 205306 (2002); Bing Dong, Ivana Djuric, H. L. Cui, and X. L. Lei, *J. Phys.: Condens. Matter* 16, 4303 (2004);
[23] Haizhou Lu, Rong Lü, and Bang-Fen Zhu, *Phys. Rev. B* 71, 235320 (2005).
[24] Zhingao Chen, Jin Wang, Baigeng Wang, and D. Y. Xing, *Phys. Lett. A* 334, 436 (2004).
[25] Ju Peng, Baigeng Wang, and D. Y. Xing, *Phys. Rev. B* 71, 214523 (2005).

FIGURE CAPTION

FIG. 1: Schematic diagram for the double AB interferometer connected with normal metal and the superconductor leads, respectively.

FIG. 2: The probability of the Andreev reflection T_{AR} vs ε in the unit of the energy gap Δ for (a) the symmetry case ($\Gamma_1^L = \Gamma_1^R = \Gamma_2^L = \Gamma_2^R = 0.02$) and asymmetry case (b) $\Gamma_1^L = \Gamma_2^L = 0.08, \Gamma_1^R = \Gamma_2^R = 0.02$, (c) $\Gamma_1^L = \Gamma_1^R = 0.08, \Gamma_2^L = \Gamma_2^R = 0.02$. The solid, dotted, dot-dashed, and dashed lines correspond to $\Omega=0, 0.02, 0.04$, and 0.08 , respectively.

FIG. 3: The magnetic flux Φ dependence of the Andreev reflection probability for $\Gamma_1^L = \Gamma_1^R = \Gamma_2^L = \Gamma_2^R = 0.02$, $\varepsilon_1 = \varepsilon_2 = 0$, $\Omega = 0.2$, and $\Phi_{12} = 0$, solid line: $\Phi = \pi/3$, dotted line: $\Phi = 2\pi/3$.

FIG. 4: The periodic oscillation of the Andreev reflection probability T_{AR} with the magnetic flux Φ ($\Gamma_1^L = \Gamma_1^R = \Gamma_2^L = \Gamma_2^R = 0.02$, $\varepsilon_1 = -0.1$, $\varepsilon_2 = 0.1$), (a) $\alpha_1/\alpha_2 = 1$. Solid line: $\Omega = 0$, $\varepsilon = 0.1$, dotted line: $\Omega = 0.05$, $\varepsilon = 0.11$, and dashed line: $\Omega = 0.1$, $\varepsilon = 0.14$. (b) $\Omega = 0.05$, $\varepsilon = 0.11$. Solid line: $\alpha_1/\alpha_2 = 2$, dotted line: $\alpha_1/\alpha_2 = 3$, and 4 for dashed line.

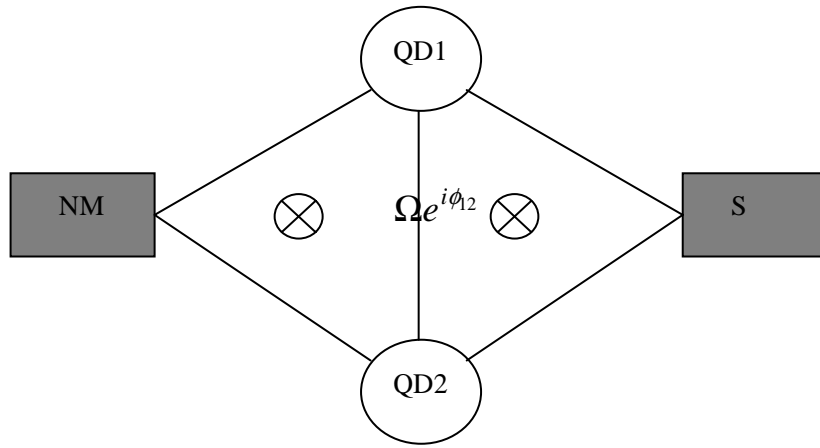
FIG. 5: Paths and corresponding phase shift. (a) for the incident electron from left lead to superconductor (b) for the reflecting hole from superconductor to left lead.

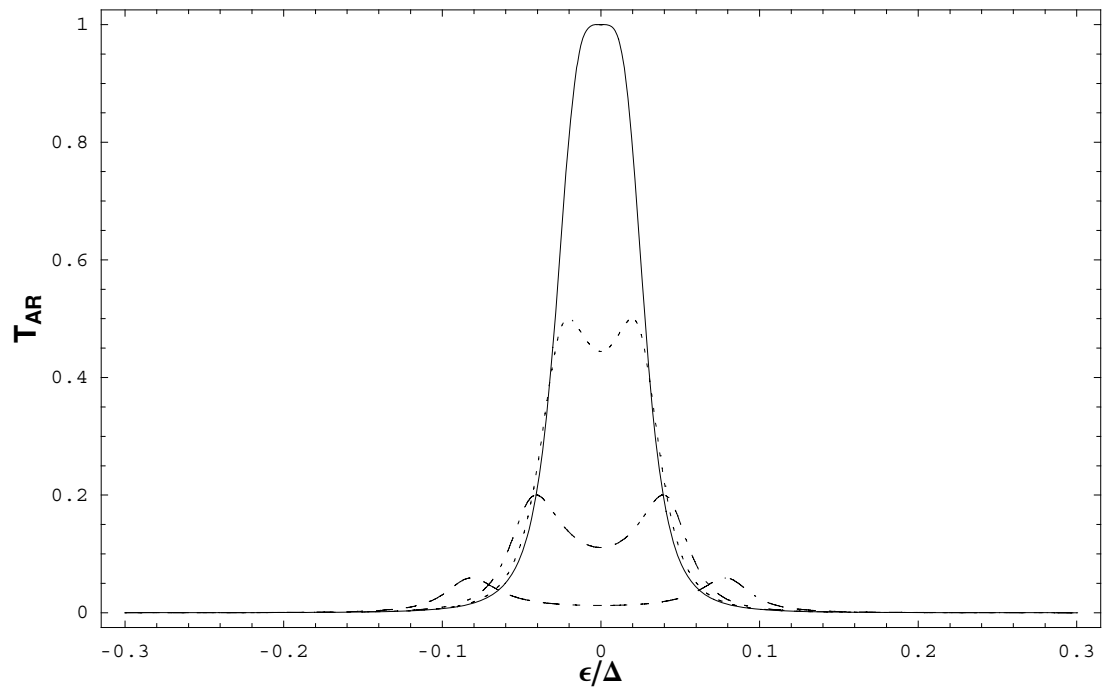
FIG. 6: Andreev reflection current J_A vs gate voltage V_g ($\varepsilon_1 = 0.1$, $\varepsilon_2 = 0.3$, $\Gamma_1^L = \Gamma_1^R = \Gamma_2^L = \Gamma_2^R = 0.02$, and $\Phi = \Phi_{12} = 0$) for bias voltage $V = 0.4$, $\Omega = 0$ (solid line), $\Omega = 0.05$ (dotted line), and $\Omega = 0.1$ (dashed line).

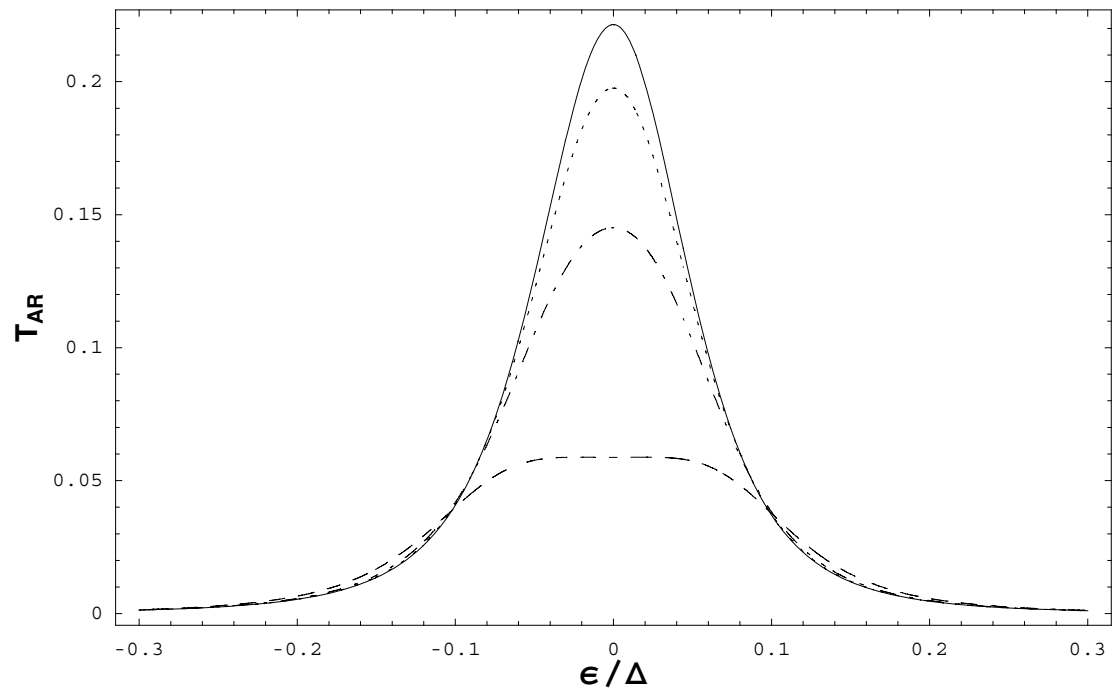
FIG. 7: Andreev reflection current vs gate voltage with the fixed total magnetic flux that $\Phi = \pi/2$ for $\Omega = 0.05$. $\Phi_{12} = 0$ (solid line), $\pi/2$ (dotted line), $3\pi/4$ (dot-dashed line), π (dashed line).

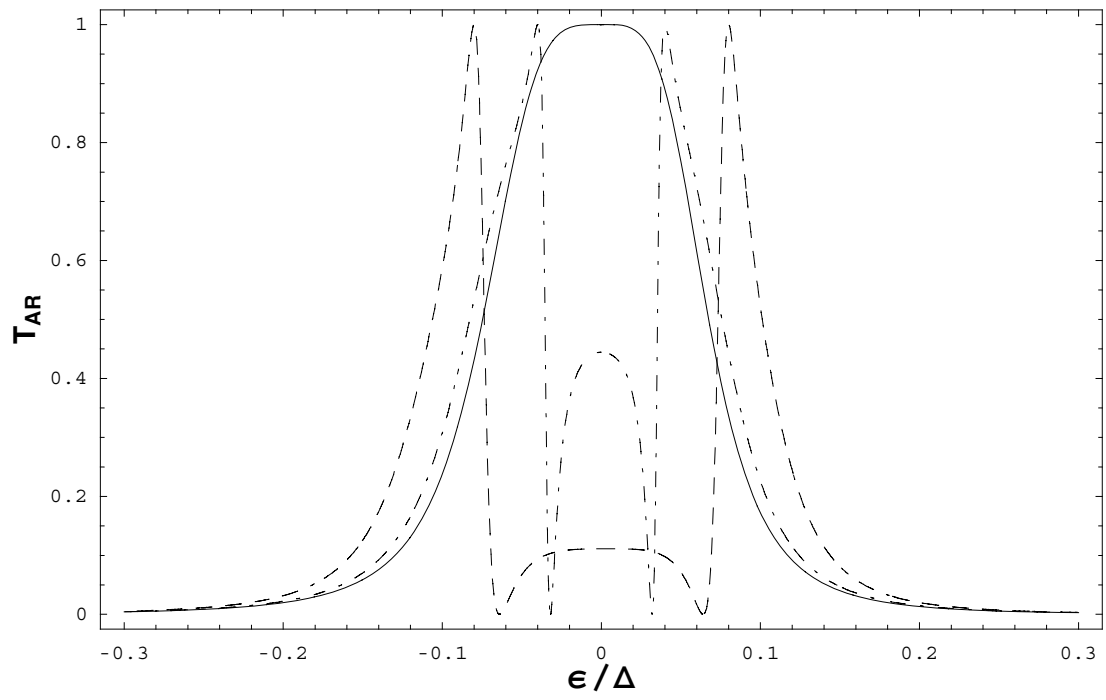
FIG. 8: Andreev reflection current vs gate voltage for $\Phi = 3\pi/2$. $\Phi_{12} = 0$ (solid line), $\pi/4$ (short-dashed line), $\pi/2$ (dotted line), π (long-dashed line).

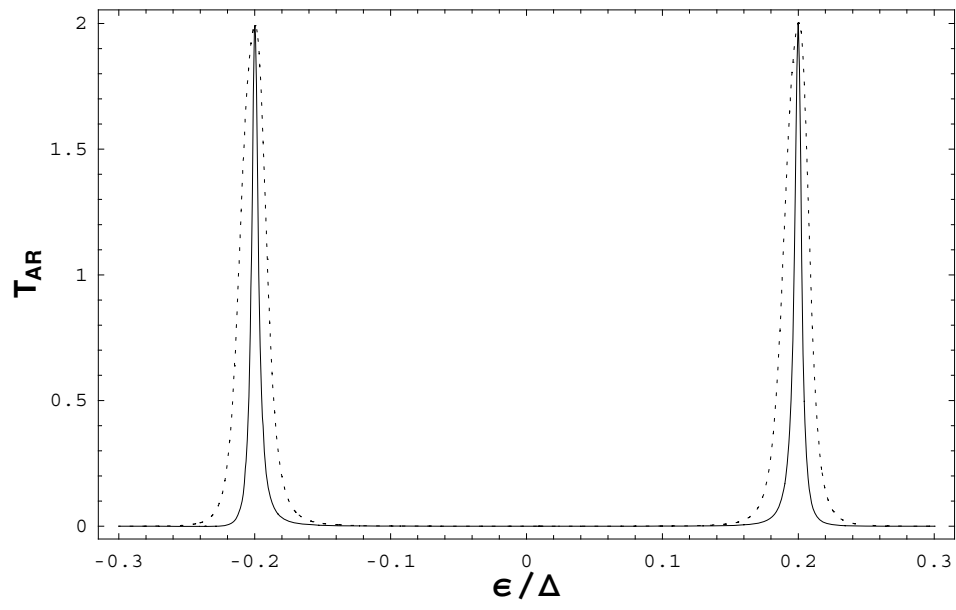
FIG. 9: Andreev reflection current vs gate voltage with $\Phi_{12} = \pi/5$ for $\Phi = 0$ (solid line), $2\pi/3$ (dotted line), $5\pi/3$ (dashed line).

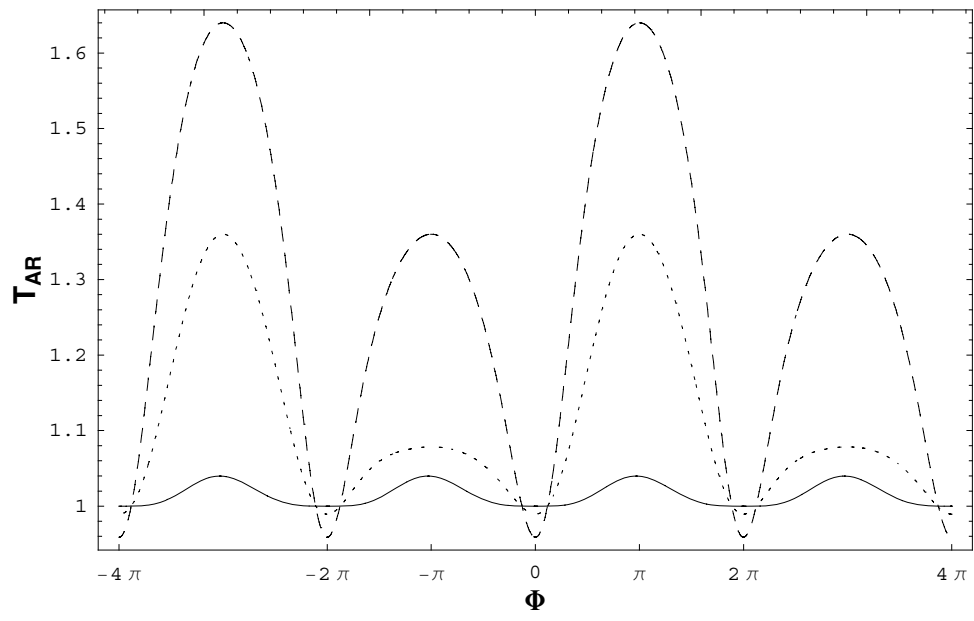


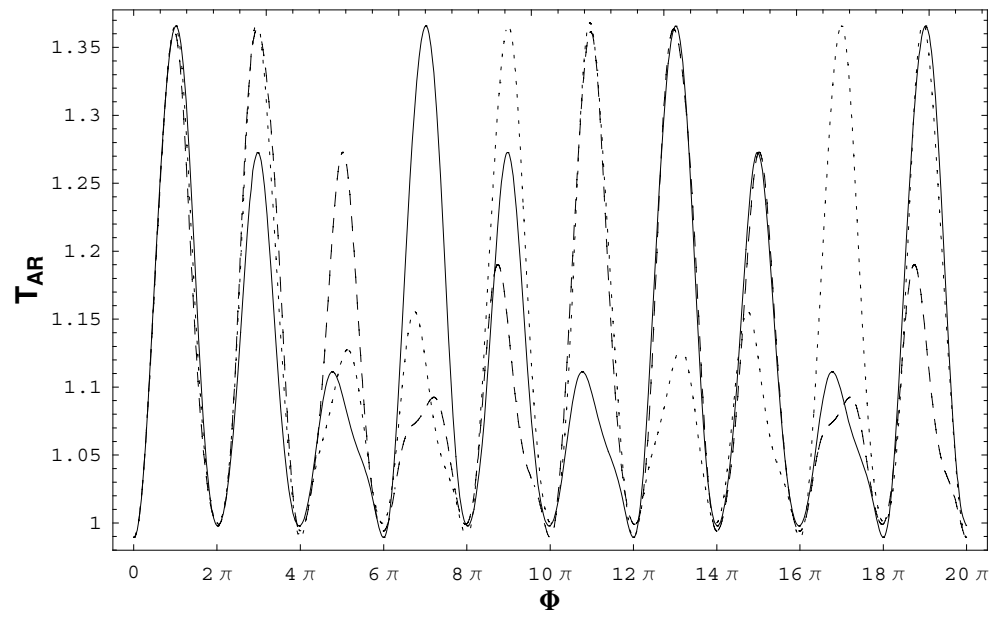


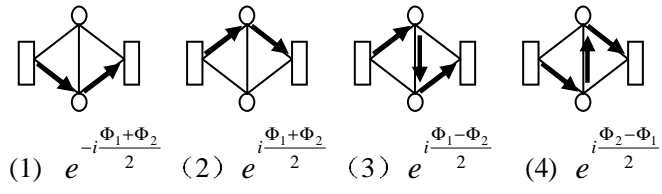




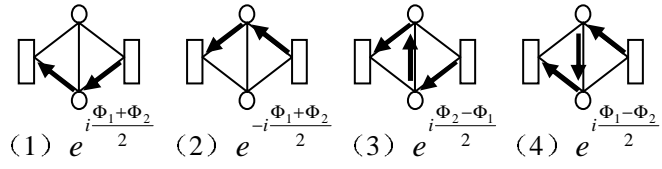








a



b

